Jornadas de Automática

RLC Circuit modelling of Magnetron Anode

Markel Larrea-Undabeitia[a,*], Joaquín Portilla[a], Jorge Feuchtwanger[a,b], Iñigo Arredondo[a], Beñat Gonzalez[a]

[a]*Department of Electricity and Electronics (EHU), Unibersitateko Errepidea, 2, 48940 Santsoena, Bizkaia.*
[b]*Ikerbasque, Basque Foundation for Science, 48009 Bilbao, Spain.*

To cite this article: Larrea-Undabeitia, M., Portilla, J., Feuchtwanger, J., Arredondo, I., Gonzalez, B. 2026. RLC Circuit modelling of Magnetron Anode. Jornadas de Automática, 47. https://doi.org/10.17979/ja-cea.2026.47.13733

Resumen

Este artículo presenta métodos para obtener circuitos equivalentes de ánodos de magnetrón mediante análisis de resonadores RLC, y posteriormente crear plantas adecuadas para el diseño de sistemas de control. Se describen dos enfoques complementarios: la extracción de parámetros del circuito equivalente a partir de la admitancia, que se obtiene de medidas de parámetros de dispersión, y el análisis de modo propio, que permite la extracción directa de las características del resonador a partir de campos electromagnéticos simulados. La validez de estos métodos se demuestra mediante su aplicación a una cavidad resonante cilíndrica simple. Posteriormente, estos métodos se aplican al análisis de un ánodo de magnetrón de 10 cavidades, demostrando cómo los parámetros del circuito equivalente dependen de la geometría del dispositivo. Los resultados obtenidos permiten modelar el comportamiento electromagnético del ánodo del magnetrón mediante un circuito equivalente, que a su vez facilita el estudio de estos dispositivos y el diseño de sistemas de control.

Palabras clave: Identificación en dominio de frecuencia, Reducción de modelos de sistemas de parámetros distribuidos, Aplicación de electrónica de potencia.

Abstract

This article presents methods for obtaining equivalent circuits of magnetron anodes through analysis of RLC resonators, and subsequently creating plants suitable for control system design. Two complementary approaches are described: extraction of equivalent circuit parameters from the admitance, which are obtained from scattering parameter measurements, and eigenmode analysis, which allows direct extraction of resonator characteristics from simulated electromagnetic fields. The validity of these methods is demonstrated through application to a simple cylindrical resonant cavity. Subsequently, these methods are applied to the analysis of a 10-cavity unstrapped magnetron anode, demonstrating how equivalent circuit parameters depend on device geometry. The results obtained enable modelling of the electromagnetic behavior of the magnetron anode through an equivalent circuit, which in turn facilitates the study of these devices and the design of control systems.

Keywords: Frequency domain identification, Model reduction of distributed parameter systems, Application of power electronics.

1. Introduction

The magnetron is a high-power vacuum oscillator that converts direct-current electrical energy into microwave-frequency electromagnetic radiation. It belongs to the family of crossed-field devices, in which a static electric field and a static magnetic field act simultaneously and perpendicularly on a dense cloud of electrons, forcing them into curved trajectories that continuously transfer energy to a surrounding resonant structure (Collins, 1948). Due to this efficient interaction mechanism, the magnetron is capable of delivering

*Corresponding author: markel.larrea@ehu.eus

kilowatts to megawatts of peak microwave power at frequencies ranging from roughly 1 GHz to 100 GHz, while remaining compact, robust, and inexpensive when compared to other microwave sources. These qualities made it the enabling technology of centimetre-wave radar during the Second World War and, decades later, the heat source inside virtually every domestic microwave oven.

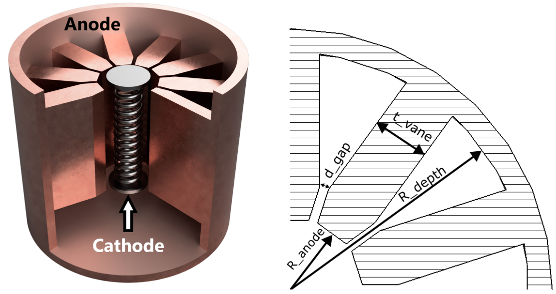

(a) (b)

Figure 1: Geometry of the magnetron.

A cylindrical thermionic cathode at the centre emits electrons radially outwards, towards a coaxial copper anode block (both shown in Figure 1(a)). A DC voltage V_a applied between cathode and anode creates a radial electric field $\mathbf{E}$, while an axial magnetic field $\mathbf{B}$, supplied by a permanent magnet or an electromagnet, is imposed along the tube axis. Electrons are subject to the Lorentz force $\mathbf{F} = q(\mathbf{E} + \mathbf{v} \times \mathbf{B})$, which curves their trajectories into cycloidal paths rather than straight radial lines (Slater, 1954). When the magnetic field exceeds the critical threshold (the Hull cut-off condition, B_c), electrons can no longer reach the anode and instead return to the cathode, a regime that defines the operating point of the device (Hull, 1921). When this condition is met, electrons form a rotating cloud that orbits the cathode. The electron trajectories and the shape of the electron cloud are shown in Figure 2.

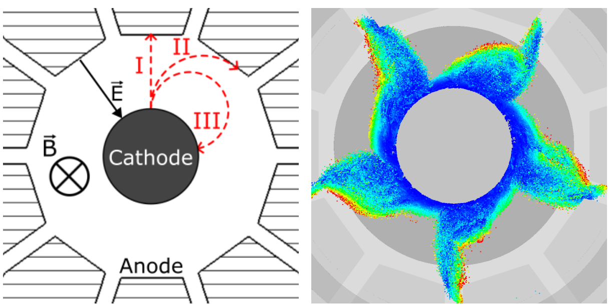

(a) (b)

Figure 2: Electron trajectories depending on the magnetic field (a) with $B = 0T$ (I), $B = B_c$ (II), and $B > B_c$ (III) and electron cloud distribution of the π-mode of a 10-vane magnetron (b).

The resonant cavities added to the anode block are what makes the oscillation mechanism work. Each cavity has a specific resonant frequency determined by its geometry, and the rotating electron cloud interacts with these cavities and excites their resonant modes. The combination of resonant cavities makes it so that many oscillating modes can be excited (Carter, 2018), but the one that is most efficiently excited is the π-mode, in which adjacent cavities are 180° out of phase.

2. Equivalent circuit of the magnetron anode

To analyse the behavior of the magnetron, it is common to use an equivalent circuit that represents each cavity as a parallel RLC circuit. Obtaining an equivalent circuit for the magnetron facilitates the understanding of its frequency response and dynamic behavior.

The anode geometry chosen to be studied is shown in Figure 1. It consists of 10 vanes that form 10 resonant cavities. The anode is not strapped, which means that there are no metallic straps connecting the vanes, as is common in some magnetron designs. These straps improve mode separation and stability of the magnetron, but they also make the equivalent circuit much more complex.

The equivalent circuit chosen to characterize the anode of the magnetron is one composed of RLC resonators connected in series to form a ring, so that each one corresponds to one of the anode cavities. The equivalent circuit with 10 RLC resonators is shown in Figure 3(b).

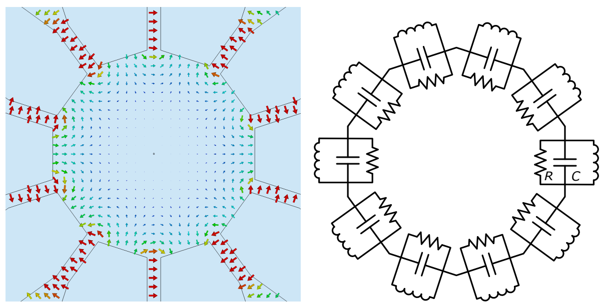

(a) (b)

Figure 3: Electric field distribution of the $\pi - mode$ (a) and equivalent circuit with 10 RLC resonators (b).

It must be noted that the equivalent circuit shown in Figure 3(b) is a simplified model of the magnetron anode, and it does not take into account all the physical phenomena like coupling between cavities or the effect of the cathode. However, it is a good starting point to understand and analyse the behavior of the magnetron.

The electric field distribution of the π-mode from which the equivalent circuit will be extracted can be seen in Figure 3(a), simulated with the electromagnetic simulation software CST (Dassault Systemes, 2026).

3. Obtaining the equivalent circuit from measurements

Most characterizations of high-frequency devices such as the magnetron are performed using scattering parameter analysis, which describes the relationship between incident and reflected waves at each port of the circuit. These measurements are made using a Vector Network Analyzer (VNA), which measures the scattering parameters over a specific frequency range.

The scattering parameters are complex numbers that represent the amplitude and phase of the reflected and transmitted waves, and the VNA obtains these parameters by emitting a known signal into the device under test and measuring the reflected and transmitted signals (Sayed and Martens, 2013).

The parameter measured with the VNA is S_{11}, which is ratio of the reflected wave to the incident wave. To explain the procedure, the equivalent circuit of the system is assumed to be a single parallel RLC resonator, and the scattering parameter S_{11} is measured through it.

There are several methods for obtaining the equivalent circuit from the S_{11} measurement, but the one that will be used in this case is the one in which the admittances are obtained from the scattering results, and from these the resistance, capacitance, and inductance of each RLC resonator are derived (Hong and Lancaster, 2001).

The resonant frequency is required to obtain the values of R, L, and C. It is the frequency at which a minimum occurs in the magnitude of S_{11}, which indicates maximum energy absorption by the system. In turn, the resonant frequency f_0 (or angular frequency ω_0) of an RLC circuit depends on its capacitance and inductance, and it can be calculated from the following formula:

$$f_0 = \frac{\omega_0}{2\pi} = \frac{1}{2\pi}\frac{1}{\sqrt{LC}} \tag{1}$$

To obtain the admittance from S_{11}, the following formula can be used:

$$Y = \frac{1}{Z_0}\frac{1 - S_{11}}{1 + S_{11}} \tag{2}$$

where Z_0 is the characteristic impedance of the measurement system. Once the admittance has been obtained, the admittance formula of a parallel RLC circuit can be used to obtain the values of R, L, and C (Pozar, 2011):

$$Y_{RLC} = \frac{1}{R} + j\left(\omega C - \frac{1}{\omega L}\right) \tag{3}$$

where ω is the angular frequency, C is the capacitance, and L is the inductance. We can separate the admittance into its real part, called conductance, and its imaginary part, called susceptance.

The resistance can be obtained directly from the real part of the admittance and that at the resonant frequency, replacing ω with ω_0 in (1), the susceptance becomes zero.

To obtain the capacitance, we can differentiate the imaginary part of the admittance with respect to frequency and evaluate it at the resonant frequency:

$$\left.\frac{d\Im[Y_{RLC}]}{d\omega}\right|_{\omega=\omega_0} = C + \frac{1}{\omega_0^2 L} = 2C \tag{4}$$

$$C = \frac{1}{2}\left.\frac{d\Im[Y_{RLC}]}{d\omega}\right|_{\omega=\omega_0} \tag{5}$$

Once the capacitance has been obtained, we can derive the inductance from the resonant frequency and (1):

$$L = \frac{1}{\omega_0^2 C} \tag{6}$$

One way to verify the validity of this method is to extract the parameters of an RLC resonator from the S_{11} results obtained through simulation (*Cmeas*, *Lmeas*, *Rmeas*) and compare the results with the values of R, L, and C that were entered into the simulation ($C = 1pF$, $L = 25nH$, $R = 50\Omega$). For this purpose, the circuit is simulated in the Advanced Circuit Design (ADS) software (Keysight Technologies, 2026), and the results and equivalent circuit parameters (obtained by numerical differentiation) are shown in Figure 4. The recovered parameters slightly differ from the original ones due to numerical error.

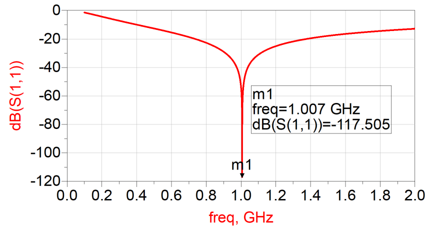

Cmeas	Lmeas	Rmeas
9.99999E-13	2.50002E-8	50.00000

Figure 4: Equivalent circuit parameters extracted from the S_{11} results in ADS (all in SI units).

In this way, the equivalent parallel RLC resonator of a system is obtained, but to obtain the equivalent circuit shown in Figure 3(b) the process is slightly different. The admittance through a parallel RLC resonator connected to other resonators forming a loop is related to the admittance of each resonator as follows:

$$Y_{measured} = \frac{N}{N-1} * Y_{RLC-cell} \tag{7}$$

where N is the number of resonators in the loop. This equation is obtained by considering the admittance of an RLC cell with $N-1$ RLC cells connected to one another in series and in parallel to the first. The results obtained for the ring of parallel RLC resonators are shown in Figure 5.

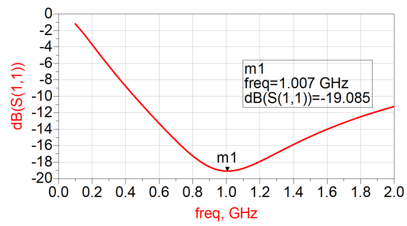

Cmeas	Lmeas	Rmeas	Ccell	Lcell	Rcell
1.25000E-12	2.00000E-8	40.00000	9.99999E-13	2.50000E-8	50.00000

Figure 5: Equivalent circuit parameters extracted from the S_{11} results in ADS, for N=5.

One can observe that the measured resistance and cell resistance, for example, follow the 4/5 ratio expected from (7).

Something that must be taken into account is that the parameters obtained for the equivalent circuit from the S_{11} measurement are dependent on port definition, and will vary with the position, orientation and impedance of the port. This is because the equivalent circuit parameters are not intrinsic properties of the system, but rather depend on how the system is excited and observed. The only parameters that are independent of the measurement method are the resonant frequency and the unloaded quality factor.

The equivalent circuit obtained from this method is better described as the circuit that represents the system's behavior at the measurement port. That is why the equivalent parameters for a single RLC resonator have been extracted from the S_{11} measurement of the magnetron anode, as considering an equivalent circuit like the one shown in figure 3(b) would not have a physical meaning.

Additionally, a python script was created that takes the S_{11} results obtained from the simulation of the magnetron anode in CST, with the port placed between two adjacent vanes, and extracts the equivalent circuit parameters. The results obtained from the simulation are compared to the results from the equivalent circuit calculated by the script in Figure 6.

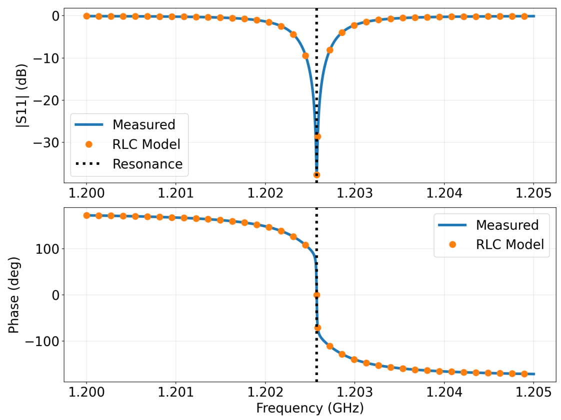

Figure 6: Comparison between simulated and RLC model S_{11} results, with C=4.13 pF, L=4.23 nH, R=112.9 kΩ.

Both the magnitude and phase of the S_{11} calculated from the extracted RLC circuit match the simulated results, thus confirming that the equivalent circuit accurately represents the system behavior as seen from the measurement port.

4. Obtaining the equivalent circuit from eigenmode analysis

This following method provides a more physically intuitive approach by extracting equivalent circuit parameters from eigenmode solutions, where the modes and frequencies (corresponding to eigenmodes and eigenvalues) at which a certain structure can resonate are computed with the Jacobi-Davidson method (Arbenz, 2016). A limitation of this method is that it must be implemented in electromagnetic solvers such as CST, HFSS, or similar tools.

By running a modal field solution in an eigenmode solver, the following parameters can be extracted directly from the computed fields (Pozar, 2011):

$$C = \frac{4\langle W_E \rangle}{V_{gap}^2} = \frac{4\langle W_E \rangle}{(E_0 \cdot d)^2} \tag{8}$$

$$L = \frac{1}{\omega_0^2 C} \tag{9}$$

$$R = \frac{\omega_0 \langle W \rangle}{P_{loss}} = \frac{Q_0}{\omega_0 C} \tag{10}$$

where $\langle W_E \rangle$ and $\langle W_M \rangle$ are the time-averaged stored electric and magnetic energies (equal at resonance), $V_{gap} = \int_0^d E_z \, dz$ is the voltage across the gap d, ω_0 is the resonant angular frequency, $\langle W \rangle$ is the total stored energy, P_{loss} is the ohmic wall loss, and Q_0 is the unloaded quality factor.

4.1. Pillbox cavity

One can check the validity of this method by simulating a simple resonant cavity like the pillbox resonator. This resonator consists of a cylindrical cavity, so the only geometric parameters that affect the resonant frequencies and modes are the radius and the height of the cylinder.

As with any other resonant cavity, more than one resonant mode can be excited in the pillbox, but the analysis will focus on the fundamental mode, which is the one with the lowest resonant frequency. This mode is the TM_{010} mode, which has an electric field distribution that is maximum at the centre of the cavity and decreases radially towards the walls. The magnetic field in this mode is purely azimuthal and also decreases towards the walls. The electric and magnetic field distributions of the TM_{010} mode in the pillbox resonator are shown in Figure 7, simulated with CST.

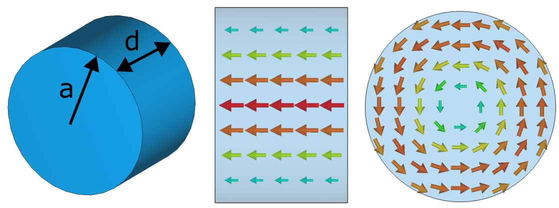

(a) (b) (c)

Figure 7: Geometry of the pillbox resonator (a), electric field (b) and magnetic field (c) distributions of the TM_{010} mode.

The resonant frequency of the TM_{010} mode in the pillbox resonator can be calculated using the following formula (Pozar, 2011):

$$f_{010} = \frac{c}{2\pi} \frac{X_{01}}{a} \tag{11}$$

where a is the radius of the pillbox, c is the speed of light in vacuum, and X_{01} is the first root of the Bessel function of order zero, which is approximately 2.405. The resonant frequency of this mode depends only on the radius of the pillbox and not on its height.

All the parameters required for the calculations in (8), (9), and (10) are given by the simulation or can be derived from the results.

The method can be validated by comparing the result for C obtained from the eigenmode analysis with the theoretical value of C, which is obtained from the analytical formula for time-averaged stored electric energy for the TM_{010} mode and (8) (Collin, 2001):

$$\langle W_E \rangle = \frac{\varepsilon_0}{4} |E_0|^2 \cdot 2\pi d \int_0^a J_0^2 \left(\frac{X_{01}}{a} r \right) r \, dr = \frac{\varepsilon_0 \pi d a^2}{4} |E_0|^2 J_1^2(X_{01})$$

$$C = \frac{\varepsilon_0 \pi a^2 J_1^2(X_{01})}{d} \tag{12}$$

where d is the height of the pillbox, ε_0 is the permittivity of free space, and $J_1(X_{01})$ is the value of the Bessel function of order one at the first root of the Bessel function of order zero.

The capacitance obtained from the eigenmode analysis is compared with the analytical formula and with the formula for the parallel plate capacitor:

$$C_{pp} = \frac{\varepsilon_0 A}{d} \tag{13}$$

where A is the area of the plates, which in this case is πa^2.

The value obtained for capacitance from the eigenmode analysis with (8) and the analytical value from (12) are both $C = 0.52pF$, while the parallel plate approximation from (13) gives a much higher value of $C_{pp} = 1.94pF$. The parallel plate formula does not take into account the fringing fields and the specific field distribution of the TM_{010} mode, as can be seen in Figure 7(b), which leads to an overestimation of the capacitance.

Once the method is validated, one can observe how the parameters of the equivalent circuit change when the geometry of the cavity is modified. As previously mentioned, the resonant frequency of the TM_{010} mode depends only on the radius of the pillbox, so by changing the height of the pillbox, the resonant frequency remains constant while the capacitance and inductance change. The results of this analysis are shown in Figure 8.

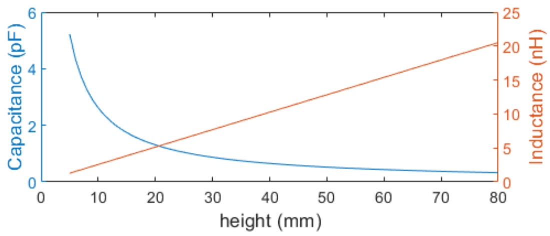

Figure 8: Capacitance and inductance of the equivalent circuit of the pillbox resonator as a function of the height of the cavity.

The capacitance of the equivalent circuit obtained from the eigenmode analysis is inversely proportional to the height, as expected from (12), while the inductance is directly proportional, also as expected from (11).

The resistance of the equivalent circuit can also be extracted from the eigenmode analysis and (10). The unloaded quality factor Q_0 obtained from the simulation was close to 40000 and constant for all heights. The results obtained for various heights match the expected behaviour from (10), and are shown in Figure 9.

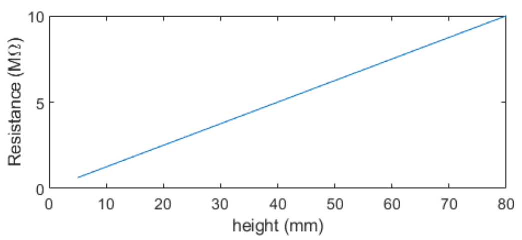

Figure 9: Resistance of the equivalent circuit of the pillbox resonator as a function of the height of the cavity.

4.2. Magnetron anode

Now that the method has been validated with a simple cavity, one can apply it to the cavities of the magnetron anode.

Same as with the pillbox, an eigenmode analysis is performed with CST and the parameters of the equivalent circuit are extracted for each of the 10 cavities. This process is more nuanced than with the pillbox, as the π-mode must be found for each geometry, and the other modes resonate with frequencies very close to the π-mode in an unstrapped magnetron.

The V_{gap} for Equation (8) is obtained by integrating the electric field along the gap between two adjacent vanes, and the electric energy in each cavity by dividing the total electric energy by 10. We get the results for various values of the gap between the vanes, which are shown in Table 1. The capacitance estimated with the parallel plate capacitor (C_{pp}) with the parallel section of the anode is also added for comparison.

Table 1: Equivalent circuit parameters for the magnetron anode cavities as a function of the gap between vanes.

g (mm)	f (GHz)	C_{pp} (pF)	C (pF)	L (nH)	R (kΩ)
1.95	1.078	2.011	4.897	4.45	112.62
2.00	1.085	1.984	4.572	4.7	120.26
2.05	1.093	1.957	3.978	5.33	138.01

Table 1 shows that this time the parallel plate approximation gives a much lower value than the one obtained from the eigenmode analysis, which could also be expected from the electric field distribution of the π-mode shown in Figure 3(a), where the electric field extends beyond the parallel section of the anode. It can also be seen that the capacitance decreases as the gap between the vanes increases.

5. Complete equivalent circuit

With the parameters of the equivalent circuit extracted from the geometry, a different equivalent circuit can be constructed, but this time including the effects of the cathode and the electron-anode interaction. This circuit is taken from (Li and Chen, 2012) and is shown in Figure 10.

In this new circuit C_2 represents the capacitance between the vanes, and L_1 the inductance, which are precisely the ones obtained from the eigenmode analysis. The need of obtaining these parameters is why the methods described are required.

The new main components of this circuit are the C_1 capacitor, which corresponds to the capacitance between the cathode and the anode, and the voltage-controlled current source, which represents the interaction of the electron cloud with the anode (connected in parallel with a current source for the noise).

Aside from these, the circuit also contains a resistance R and an additional current source. The resistance R is related but not the same as the one obtained for the equivalent RLC, as this circuit is configured differently. The current source represents an external signal that could be injected into the system, mainly used for signal control.

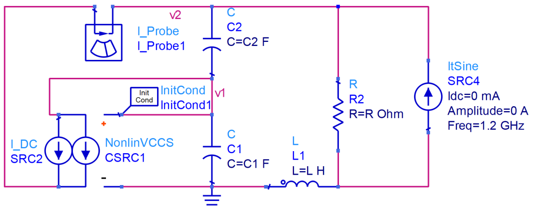

Figure 10: Equivalent circuit used for the dynamic analysis.

The current source representing the interaction of the electron cloud with the anode depends on the voltage between the cathode and the anode (which is the same as the voltage across C_1) following the following formula:

$$I = a_0 + a_1 V + a_2 V^2 + a_3 V^3 \tag{14}$$

where a_0, a_1, a_2, and a_3 are coefficients that are adjusted to match the electron-anode interaction. This is obtained from a third order Taylor series expansion of the current centred around the operating point of the magnetron.

We choose the values for the cathode-anode capacitance, the resistance and the correct source coefficients so that the circuit oscillates the expected way (rise time, saturation, output voltage and current, etc.). The noise and injection sources are ignored for now but are needed for control design. The results obtained from the transient analysis of the circuit are shown in Figure 11.

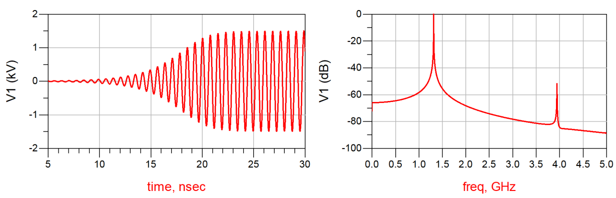

Figure 11: Transient response of the complete equivalent circuit.

The results show that the circuit oscillates at a frequency close to the expected one from the extracted capacitance and inductance. As demonstrated in (Li and Chen, 2012), this circuit can be used to analyse the dynamic behaviour of the magnetron, such as stability of the oscillation, but it can also be used to analyse the effect of geometric variations on the performance of the magnetron as well as the effect of an external signal injected into the system. These make the complete circuit a suitable plant for the design of a control system.

6. Conclusions

This work has presented two complementary methodologies for extracting equivalent RLC circuits from magnetron anode cavities: one based on scattering parameter measurements or simulations and another based on eigenmode analysis of electromagnetic field simulations. The eigenmode analysis approaches has been validated through application to a simple cylindrical resonant cavity (pillbox resonator), where agreement between analytical and extracted circuit parameters was demonstrated. The measurement-based method provides practical access to equivalent circuit parameters from real or simulated devices, while the eigenmode analysis method offers a more physically intuitive but simulation-exclusive framework. The application of both methods to a 10-cavity unstrapped magnetron anode demonstrates how equivalent circuit parameters depend sensitively on device geometry.

The results obtained in this study enable the rapid electromagnetic characterization and modelling of magnetron anodes through equivalent circuits, facilitating the analysis and optimization of microwave generation devices. These methods are particularly valuable for understanding how geometric variations affect device performance and for rapid design iteration cycles.

The extraction of capacitance and inductance also allow for the construction of more complex equivalent circuits suitable for dynamic analysis. The complete circuit presented incorporates the effects of the cathode-anode interaction and can be used as a plant model for the creation and design of control systems for magnetrons, which are common in applications such as radar and linear accelerators.

Future work should explore the extension of these methodologies to strapped anodes, including the effects of inter-cavity coupling through metal straps. Additionally, the comparison of extracted circuit parameters across different frequency bands and operating regimes would provide deeper insights into the generalizability and limitations of the equivalent circuit representation for complex magnetron geometries.

Acknowledgements

Project PID2023-148792OB-I00 funded by MICIU/AEI /10.13039/501100011033 and by FEDER, UE.

This project received funding from the European Union's Horizon Europe Research and Innovation Programme under CA No 101290927.

The authors acknowledge the use of AI-based tools for assistance in editing, grammar enhancement, and spelling checks during the preparation of this manuscript.

References

Arbenz, P., 2016. Lecture Notes on Solving Large Scale Eigenvalue Problems. ETH Zürich, Ch. 12: The Jacobi-Davidson Method.

Carter, R. G., 2018. Microwave and RF Vacuum Electronic Power Sources. The Cambridge RF and Microwave Engineering Series. Cambridge University Press.
DOI: 10.1017/9780511979231

Collin, R. E., 2001. Foundations for Microwave Engineering, 2nd Edition. IEEE Press Series on Electromagnetic Wave Theory. Wiley-IEEE Press.

Collins, G. B., 1948. Microwave Magnetrons. Vol. 6 of MIT Radiation Laboratory Series. McGraw-Hill, New York.

Dassault Systemes, 2026. CST Studio Suite.

Hong, J. S., Lancaster, M. J., 2001. Basic Concepts and Theories of Filters. John Wiley & Sons, Ltd, Ch. 3, pp. 29–76.
DOI: 10.1002/0471221619.ch3

Hull, A. W., 1921. The magnetron. Journal of the American Institute of Electrical Engineers 40 (9), 715–723.
DOI: 10.1109/JoAIEE.1921.6594005

Keysight Technologies, 2026. Advanced Design System (ADS).

Li, D., Chen, X., 03 2012. Study of nonlinear dynamics in magnetron by using circuitry model. Physics of Plasmas 19.
DOI: 10.1063/1.3694843

Pozar, D. M., 2011. Microwave Engineering, 4th Edition. Wiley, Hoboken, NJ.

Sayed, M., Martens, J., 2013. Vector network analyzers. The Cambridge RF and Microwave Engineering Series. Cambridge University Press, p. 98–129.

Slater, J. C., 1954. Microwave Electronics. D. Van Nostrand, Princeton, NJ.